



HAL
open science

Thermal and energy analysis of mechanical spectrometry tests

André Chrysochoos, Olivier Arnould

► **To cite this version:**

André Chrysochoos, Olivier Arnould. Thermal and energy analysis of mechanical spectrometry tests. 2022. hal-03697346v1

HAL Id: hal-03697346

<https://hal.science/hal-03697346v1>

Preprint submitted on 16 Jun 2022 (v1), last revised 10 Mar 2023 (v3)



HAL is a multi-disciplinary open access archive for the deposit and dissemination of scientific research documents, whether they are published or not. The documents may come from teaching and research institutions in France or abroad, or from public or private research centers.

L'archive ouverte pluridisciplinaire **HAL**, est destinée au dépôt et à la diffusion de documents scientifiques de niveau recherche, publiés ou non, émanant des établissements d'enseignement et de recherche français ou étrangers, des laboratoires publics ou privés.



Distributed under a Creative Commons Attribution 4.0 International License

Thermal and energy analysis of mechanical spectrometry tests

 André Chrysochoos and  Olivier Arnould

Laboratoire de Mécanique et Génie Civil, Université de Montpellier, CNRS, Montpellier, France

Quantitative infrared techniques were developed and used to assess small temperature variations of samples undergoing cyclic loadings during mechanical spectrometry tests. A standard setup of dynamic mechanical thermal analysis (DMTA) was therefore modified for this purpose. Thermal and mechanical data were used to quantify the viscous dissipated and the thermoelastic coupling energies that can be both associated with the hysteretic stress-strain response of polymers. Energy balances were then performed to quantify the relative importance of dissipative and thermoelastic coupling heat sources. The consequences of the obtained results on the identification of the material rheological properties within a linear viscoelastic framework were finally discussed.

Keywords DMTA, viscous dissipation, thermoelastic coupling, energy balance, time-dependent behavior

1 Introduction

DMTA is widely used in standard experimental approaches developed to characterize the linear viscoelastic behavior of polymers. Samples are subjected to a monochromatic sinusoidal loading (e.g., in tension-compression) and the stress-strain response is recorded at different environmental chamber temperature T_0 and loading frequency f_0 , to derive the so-called dynamic moduli E' and E'' . According to the hypotheses of DMTA, the storage modulus E' is linked to the stored elastic energy, finally mechanically recoverable when the specimen is unloaded, while the loss modulus E'' is related to the viscous dissipated energy over a loading cycle. In the literature, the viscous part of the behavior is equally quantified by the loss angle δ , defined by $\tan \delta = \frac{E''}{E'}$, which characterizes the so-called internal friction (Menard 2008). The DMTA rheological equations for strain-controlled tensile loading can be gathered as follows:

$$\begin{cases} \varepsilon = \varepsilon_0 \sin \omega_0 t, & (1a) \end{cases}$$

$$\begin{cases} \sigma = \sigma_0 \sin (\omega_0 t + \delta) = E' (T_0, f_0) \varepsilon_0 \sin \omega_0 t + E'' (T_0, f_0) \varepsilon_0 \cos \omega_0 t, & (1b) \end{cases}$$

$$\begin{cases} E' (T_0, f_0) = \frac{\sigma_0}{\varepsilon_0} \cos (\delta (T_0, f_0)), & (1c) \end{cases}$$

$$\begin{cases} E'' (T_0, f_0) = \frac{\sigma_0}{\varepsilon_0} \sin (\delta (T_0, f_0)), & (1d) \end{cases}$$

where, ε_0 stands for the controlled strain amplitude, $\sigma_0 (T_0, f_0)$ the resulting stress amplitude and $\omega_0 = 2\pi f_0$ the pulsation.

Eqs. (1a) to (1d) form the theoretical interpretation framework of DMTA. They deserve several comments:

- The mechanical spectrometry tests assume that to a monochromatic mechanical loading corresponds a monochromatic response. Naturally, this crucial preliminary assumption can/should be systematically verified via a frequency spectrum analysis of the loading signal and of the material response. The two questions that need to be imperatively answered are: is the testing machine capable of imposing a monochromatic loading? Is the material response then also monochromatic?
- Moreover, although tests are performed at different temperatures, they are generally considered isothermal, the sample being assumed to be in thermal equilibrium with the

environmental chamber. However, the cyclic deformation mechanisms of polymers often lead to temperature variations of the specimen. Material deformation process generates indeed heat sources. Dissipative sources induced by irreversible transformations, due at least to viscosity, must be first mentioned. In addition, it is known that polymer behaviors are sensitive to temperature variations. This sensitivity results in coupling mechanisms, highlighting the strong dependence between thermal, mechanical, and microstructural states. One can mention the linear thermal expansion of polymers (Graessley et al. 2001), the rubber effects (Treloar 2005), or simply the fact that elastic moduli vary with temperature (e.g., the temperature T_0 of the DMTA environmental chamber) (Menard 2008; Ferry 1980). Consequently, are the temperature variations of the sample undergoing DMTA testing significant or not? If so, a better understanding of the energy balance of the polymer deformation is then interesting from a rheological standpoint, dissipative mechanisms being closely associated with evolution laws, while coupling effects are linked to state laws (Halphen et al. 1975; Chrysochoos 2012).

The first goal of this paper is to present the thermography setup used to assess very small strain-induced temperature variations occurring during cyclic DMTA tests. As already mentioned, DMTA performs isothermal analysis even if different testing temperatures are, by construction, considered in testing campaigns. This isothermal analysis was reconsidered to check whether the origin of the storage and loss moduli is only due to visco-elastic effects whatever the couple (T_0, f_0) . In the following, metrological aspects related to measurements of small temperature variations were thoroughly presented. Indeed, the first experimental challenge was to measure these strain-induced temperature variations. Even if these temperature variations remain often much smaller than a tenth of a degree, they may correspond to heat rates much greater (e.g., dozens of times) than the deformation energy rate (Boulanger et al. 2004). It is therefore important not to neglect them when establishing the energy balance.

2 Experimental setup

The chosen polymers in this study were commercial PS (Polystyrene from Goodfellow) and commercial PA6.6 (Polyamide 6.6). PA6.6 samples were provided by Solvay Engineering Plastics, for which the authors are gratefully acknowledged. The specimens of dimension $85 \times 13 \times 4 \text{ mm}^3$ were machined from thick sheets of $300 \times 300 \text{ mm}^2$. Note that the glass transition temperature (T_g) is around 375 K for PS and 336 K for PA6.6.

2.1 Thermal metrology

Temperature variations were observed using an infrared focal plane array (IRFPA) camera (CEDIP Titanium series). The environmental chamber of the DMTA (Bose ELF 3230) was equipped with a home-made door using an infrared Techspec lens, from EDMUND optics, and placed at the center of the door. This infrared lens was made of anti-reflecting coated silicon to avoid IR reflections and was suitable for the DMTA measurements in the wavelength range of $3\text{-}5 \mu\text{m}$ (transmission coefficient of IR radiations in this range remains greater than 93%).

This infrared lens was thus able to capture the temperature variations observed during the tests by weakly attenuating them. The experimental setup is shown in Figure 1. Furthermore, two samples were placed inside the environmental chamber, in the optical field of IRFPA camera and at the same focal plane, one sample being subjected to the loading and the other one mechanically free (dummy sample) and submitted to the thermal regulation of the environmental chamber (Figure 2).



Figure 1: Thermography setup in front of the DMTA (BOSE ELF 3230)

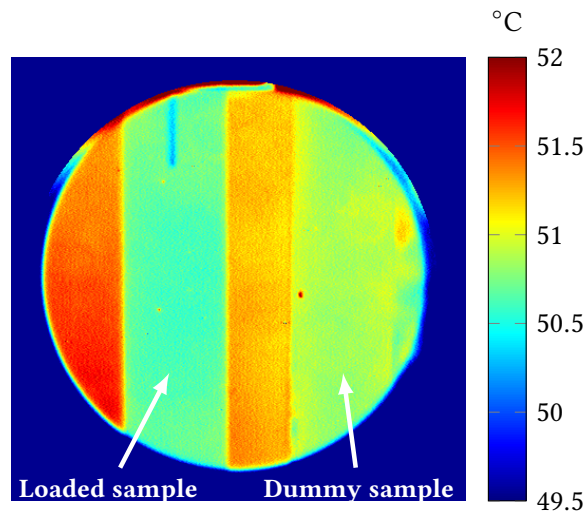


Figure 2: Thermal image (in °C) of the two PS samples inside the environmental chamber at 50 °C

The IRFPA camera was calibrated using a pixel-by-pixel method [Honorat et al. \(2005\)](#). This pixel calibration is an effective technique for quantitatively reliable infrared measurements of temperature fields, particularly when very small temperature variations occur. This type of calibration allows the user to by-pass the “bad pixel replacement” (BPR) and “non uniformity correction” (NUC) stages proposed by some camera’s builders. The individual pixel calibration is done on the entire dynamic range of the sensor and is based on polynomial fitting of the digital levels s_i delivered by the i^{th} element of the detector matrix when the camera is placed in front of a black body source at different temperatures $T \in [T_1, T_2]$:

$$s_i(T) = \sum_{p=0}^P a_{ip} T^p, \text{ for } T \in [T_1, T_2]. \quad (2)$$

The coefficients noted a_{ip} in Eq. (2), derive from a least squares fitting. Later, the system will consider pixel i as a bad pixel based on the temperature difference between the temperature predicted by the polynomial fitting and the imposed temperature of the black body source. If

this difference is greater than a predefined threshold of δT (e.g., $\delta T = 10$ mK), then the pixel is considered as bad (Honorat et al. 2005).

This calibration procedure was adopted for each testing temperature T_0 used to ensure that very small strain-induced temperature variations of the sample are measured. Calibrations were performed before each mechanical test series, using the black body behind the environmental chamber's door with the IR lens and using the same geometrical configuration as during the DMTA test, the surface of the black body being at the same position as the sample surface. The integration time was varied according to the temperature used during the DMTA tests. To avoid transient thermal drifts of the camera, these calibrations and measurements were performed about 4-5 hours after switching on the camera.

A tricky recurrent problem associated with the IR thermal measurements is the emissivity of the target, here the emissivity of the sample surface. It was verified whether painting the sample black, will affect the emissivity of the sample, as some samples (PS) were transparent to the visible radiations. Therefore, half of one PS sample was painted black and half of it was left unpainted. Using the experimental setup shown in Figure 1, thermoelastic responses were analyzed over the sample gauge part to check if painting the sample black makes a difference in the emissivity (in the IR wavelengths) of the sample. The thermoelastic field of temperature amplitudes was plotted over the region of interest including both sides (i.e., painted and unpainted). It was observed that painting the sample in black induced a more homogeneous thermoelastic signal but did not significantly affect its mean amplitude $\delta\theta_e^{f_0}$ over the sample gauge part (see its definition in subsection 3.2). We consequently decided to leave the sample surfaces unpainted.

2.2 Mechanical loadings

Regarding now the loading aspects of the cyclic tests, we limited the mechanical tests to three decades of loading frequencies for different environmental chamber's temperatures, all below the glass transition temperature T_g to limit the complexity of the behavior to that of glassy polymers.

In this work, a complete calibration of the load cell and of the LVDT displacement sensor were performed. Moreover, the alignment of the clamps was verified and adjusted to ensure a pure tensile loading of the sample. For this purpose, we used a PS sample equipped with four strain gauges, two by side, to verify if the strain is (almost) equal for all the four gauges for different applied quasistatic load in tension and compression until the maximum load. In addition, the DMTA electronic acquisition chain influenced the phase shift between the imposed displacement and the measured force. This phase shift was corrected in the (commercial) software but, as we used the raw data to fully control the data processing and to synchronize these signals with the IR camera acquisition, an electronic phase shift correction has been done on the raw data. This phase shift has been evaluated at all the measured frequencies and at two temperatures (28 °C and 60 °C using a sample of steel (no material viscosity) sheet. This steel sheet was of the same length as the polymer samples but with a cross-section area such that it has a stiffness equivalent to that of PS samples. Finally, regarding the real sample elongation, it was considered that components of the DMTA machines (especially the load cell) induced a non-negligible spurious displacement that induced an important bias. Therefore, the machine stiffness was measured using a very stiff sample. The actual elongation of the sample was then obtained by correcting the machine displacement from its own deformation. This was checked by measuring the actual displacement, during cyclic loadings, between two targets on the surface of a polymer sample by digital image correlation (Wattrisse et al. 2001) using IR thermal images. The polymer samples complex stiffness was then corrected following the equation (16A) in Olusanya (1996). The moduli determined on the PS and PA6.6 samples were compared with measurements obtained on similar samples using other DMTA in three other French laboratories (Yadav 2019).

The raw displacement and load measurements of the DMTA were used to verify the monochromatic character of the loading and response signals. An example of the Fourier spectrum of the raw force and displacement signals, recorded on a PS sample at 1 Hz, is shown in Figure 3.

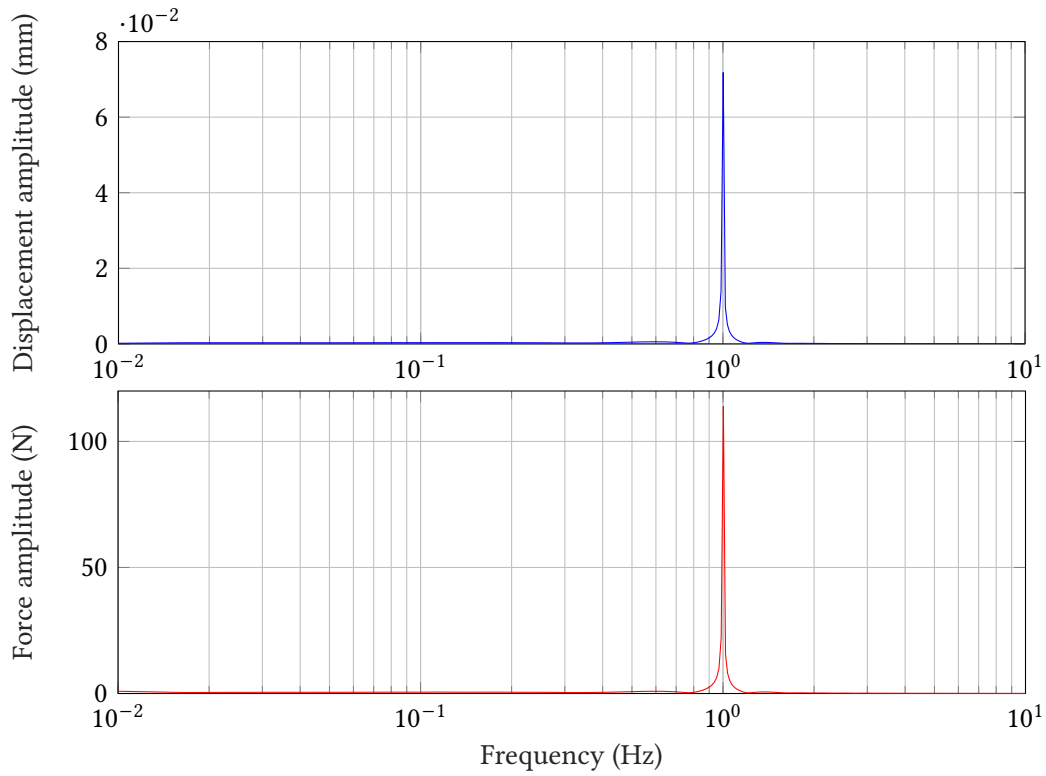


Figure 3: Frequency spectrum of the force and displacement signals for PS sample at a loading frequency of 1 Hz and a temperature of 40 °C

This type of control was performed on all samples, regardless of the loading frequency f_0 or the ambient temperature T_0 at which the test was performed. Strain controlled tension-compression symmetric cyclic measurements were conducted on specimens at several frequencies (e.g., 0.01, 0.1, 1 and 10 Hz) and several temperatures. The following sets of T_0 have been particularly analyzed: (313 K, 348 K, 363 K) for the PS samples and (313 K, 323 K, 333 K) for the PA6.6 samples.

The recordings were made over several tens of cycles to get a stabilized cyclic regime and ensure a sufficient set of mechanical and thermal data to perform relevant filtering. We used the same sampling frequency whatever the loading parameters and the polymer tested. This mechanical sampling frequency f_s was set at 31 Hz, as a unique electronic sampler being used to record thermal and mechanical data synchronously. This frequency is large enough for loading frequencies below 1 Hz. In fact, whatever the frequency, the expected periodicity of the signal, once the transient period is over, allowed us to analyze the thermal response via synchronous demodulation techniques. In addition, the sampling frequency of 31 Hz was chosen so as not to be an integer multiple of the high loading frequencies used of 6.3 and 10 Hz (under-sampling technique).

The loading parameters used during the different tests are mentioned in Table 1.

	Polystyrene	Polyamide 6.6
Max. strain	0.1%	0.1%
Strain ratio	-1	-1
Freq. range	[0.01-10] Hz	[0.01-10] Hz
Temp. range	[313-363] K	[308-333] K

Table 1: Loading parameters of DMTA tests

3 Results and Discussion

The results obtained were processed separately: on the one hand, mechanical data (load, displacement, time) led us to identify dynamic moduli (see Eqs. (1c) and (1d)) as functions of the testing temperature T_0 and of the loading frequency f_0 ; on the other hand, IR data gave us the temperature variations of the specimen inside the environmental chamber due to the cyclic loading.

3.1 Estimates of dynamic moduli E' and E''

Classically, DMTA is used to identify the evolution of dynamic moduli. All devices directly provide E' and E'' moduli (or equivalently E' and $\tan \delta$), as they are equipped with a specific processing data software. In the present case, we decided to process the raw stress and strain data recorded as a function of time, the dynamic moduli have thus been estimated using a simple least-squares method of the stress and strain signals.

Series of frequency sweeps gave the evolution of E' and E'' shown in Figures 4 and 5 and presented as functions of the loading frequency f_0 and environmental chamber temperature T_0 . These data were extracted from Yadav's works during his PhD (Yadav 2019).

It was observed that the evolution of E' and E'' have the same trends for both materials (PS and PA6.6): for the used frequency range, E' is increasing with the increasing frequency whereas E'' is decreasing. On the other hand, an increase in the testing temperature will tend to decrease the storage modulus and increase the loss modulus. Finally, it is worth mentioning the difference in order of magnitude between E' and E'' , loss moduli being, roughly speaking, dozens of times weaker than storage moduli.

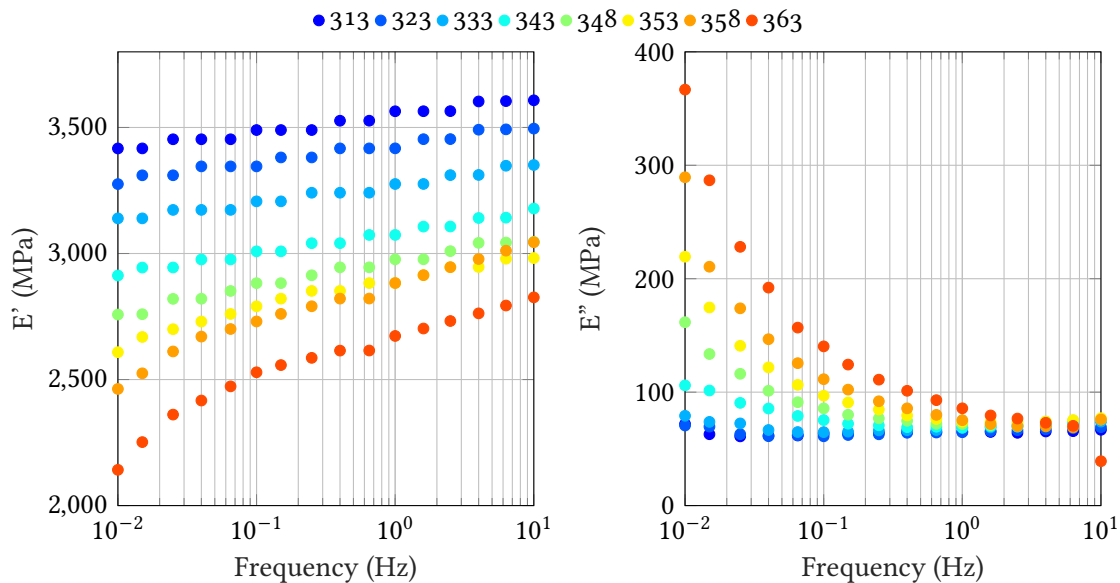


Figure 4: Influence of frequency and temperature on dynamic moduli of PS, after Yadav (2019); colors indicate the temperature T_0 in K of the environmental chamber

Naturally, this type of result is very common in the literature and widely used in the polymer material characterization centers to construct master curves associated with the famous, and sometimes controversial, time-temperature superposition principle (Sokolov et al. 2007). However, if the mechanical data from DMTA tests are abundant, the associated thermal responses have not, to our knowledge, been analyzed yet. This is probably not surprising since, as previously underlined, one of the implicit assumptions of DMTA tests is to consider that the sample is in thermal equilibrium with the environmental chamber inside which it is cyclically loaded.

3.2 Analysis of temperature variations

To estimate the so-called "temperature variations of the sample" $\theta(t)$, we used the infrared techniques presented in subsection 2.1. These temperature variations were defined by the

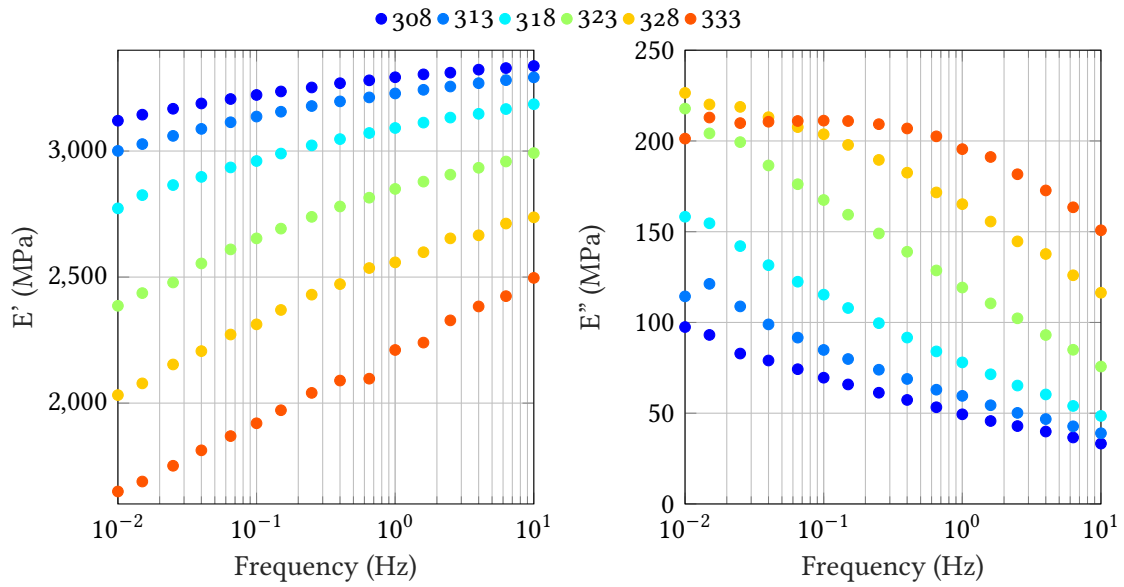


Figure 5: Influence of frequency and temperature on dynamic moduli of PA6.6, after [Yadav \(2019\)](#); colors indicate the temperature T_0 in K of the environmental chamber

difference between the average temperatures estimated over two small areas of $2 \times 2 \text{ mm}^2$ placed, one in the center of the sample being deformed and, the other, in the center of the dummy sample. The purpose of calculating an average temperature over a small area is to reduce high frequency thermal noise. For the IRFPA camera used in this work, this noise is white Gaussian noise ([Chrysochoos et al. 2000](#); [Batsale et al. 2013](#)). Considering the temperature difference between the strained sample and the dummy sample is intended to mitigate the effects of low frequency temperature fluctuations in the environmental chamber induced by its own thermal regulation system.

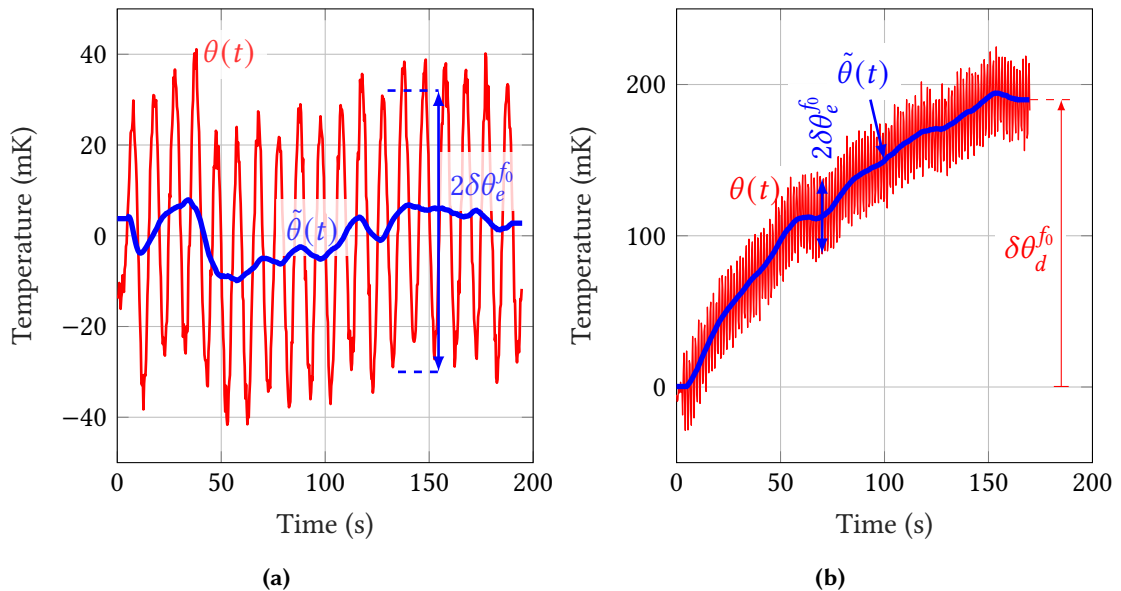


Figure 6: Time courses of $\theta(t)$: (a) PA6.6, $T_0 = 313 \text{ K}$, $f_0 = 0.1 \text{ Hz}$; (b) PA6.6, $T_0 = 333 \text{ K}$, $f_0 = 10 \text{ Hz}$

Figures 6(a) and 6(b) present the temperature $\theta(t)$ obtained on PA6.6 samples. To fix the ideas we have chosen the couples (313 K, 0.1 Hz) and (333 K, 10 Hz) representing the extreme conditions of mechanical and thermal loading for the polyamide samples.

The red curve shows the evolution of $\theta(t)$ while the blue curve represents the evolution of the mean temperature per cycle $\tilde{\theta}(t)$ defined by:

$$\tilde{\theta}(t) = f_0 \int_{t-(2f_0)^{-1}}^{t+(2f_0)^{-1}} \theta(\tau) d\tau. \quad (3)$$

The difference $\theta(t) - \tilde{\theta}(t)$ makes it possible to highlight regular and periodic oscillations whose amplitude has been noted $\delta\theta_e^{f_0}$. We finally introduced the temperature difference $\delta\theta_d^{f_0}$ defined by:

$$\delta\theta_d^{f_0} = \tilde{\theta}(t_{end}), \quad (4)$$

where t_{end} is the end time of the camera recording. This temperature allowed us to quantify a potential self-heating of the sample induced by viscous dissipation. However, the value of $\delta\theta_d$ can be affected by the residual temperature fluctuations of the environmental chamber.

These first thermal data allowed us to point out the two following results:

- First, we observed that the temperature variations during the DMTA test remained very small (less than a few hundreds of mK). On the one hand, this result is reassuring in that it is consistent with the assumption of a DMTA test during which the sample is in thermal equilibrium with the ambient temperature of the environmental chamber. On the other hand, one could be surprised not to see much more significant dissipation-induced self-heating. In the case of Figure 6(a), the loading frequency is low (0.1 Hz) and no significant $\delta\theta_d$ is observed. However, in the case of Figure 6(b), PA6.6 sample is cyclically loaded at 10 Hz at a temperature of 333 K, the temperature increase $\delta\theta_d$ does not exceed 200 mK during the test duration. In the next subsections we checked whether this observation is consistent with the temperature variations induced by viscous dissipation predicted by the rheological equations Eqs. (1).
- Even if variations of $\theta(t)$ are small, regular oscillations can be observed which appears to be periodic, and this periodicity is linked to the loading frequency f_0 . We noted $\delta\theta_e^{f_0}$ the amplitude of these oscillations and we proposed to associate them with thermoelastic effects. In the next subsection, a thermoelastic rheological equation was introduced to check this proposal.

3.3 Thermodynamic standpoint and energy balance analysis

To go further, it is necessary to consider the 1D rheological equations associated with the DMTA tests and try to integrate them in a thermodynamic framework to be able to draw up a complete energy balance. In this work, the thermodynamics of irreversible processes (TIP) with internal state variables was used (Halphen et al. 1975; Germain et al. 1983; Chrysochoos 2012). This formalism assumes that a local equilibrium state exists and that it can be described by a finite number of state variables. The properties of equilibrium states are described by the state laws derived from a thermodynamic potential. In mechanics of materials, the volume Helmholtz free energy ψ is often used. The state variables are the temperature T , the small strain ε and a given number of complementary (internal) state variables α_j , $j = 1, 2 \dots$, usually introduced to describe the microstructural state of the material. Evolution or complementary equations must also be introduced to describe the irreversibility accompanying the deformation process. The latter must be compatible with the Clausius-Duhem inequality, local writing of the 2nd principle of thermodynamics (Chrysochoos 2012).

Using the rheological Eqs. (1) associated with the DMTA tests, the stress σ can be rewritten in the following form, easier to interpret from a thermodynamic standpoint:

$$\sigma = E'(T_0, f_0)\varepsilon + \frac{E''(T_0, f_0)}{2\pi f_0} \dot{\varepsilon}. \quad (5)$$

The energy denomination of E' and E'' allows one to split the stress into reversible (energy storage or conservation) and irreversible (loss of energy) parts so that:

$$\begin{cases} \sigma^r = \frac{\partial \psi}{\partial \varepsilon} = E'(T_0, f_0)\varepsilon, & (6a) \\ \sigma^{ir} = \sigma - \sigma^r = \frac{E''(T_0, f_0)}{2\pi f_0} \dot{\varepsilon}. & (6b) \end{cases}$$

The conjugate variable of ε is the so-called reversible stress σ^r . The term σ^{ir} is the irreversible stress and will act as the thermodynamic force associated with the strain rate in the Clausius-Duhem inequality (see subsection 3.3.2).

The presence in Eqs. (6a) and (6b) of the thermomechanical loading parameters T_0 or f_0 is a little bit delicate to integrate in a thermodynamic framework. How can these (external loading) parameters act as material state variables ?

Regarding T_0 , it is quite simple, just replace the temperature set point of the environmental chamber by the temperature of the sample T .

Regarding f_0 , we proposed the following state variable \tilde{f} , depicting a memory of kinematic effects cumulated over a time corresponding to a loading duration \mathcal{T}_0 :

$$\tilde{f} = \frac{1}{2\pi} \sqrt{\frac{\langle \dot{\varepsilon}^2 \rangle}{\langle \varepsilon^2 \rangle}}, \quad (7)$$

with the mean square strain rate over \mathcal{T}_0 defined by $\langle \dot{\varepsilon}^2 \rangle = \frac{1}{\mathcal{T}_0} \int_{t-\mathcal{T}_0}^t \dot{\varepsilon}^2(\tau) d\tau$ and the mean square strain $\langle \varepsilon^2 \rangle = \frac{1}{\mathcal{T}_0} \int_{t-\mathcal{T}_0}^t \varepsilon^2(\tau) d\tau$. Naturally, when \mathcal{T}_0 corresponds to the cycle period f_0^{-1} , all is done to get $\tilde{f} = f_0$ for a monochromatic loading cycle.

In what follows, we therefore admitted that the free energy ψ was a state function of T , ε and of the history variable \tilde{f} so that $\psi = \psi(T, \varepsilon, \tilde{f})$.

The form of Eq. (5) suggests a rheological behavior where elastic effects develop in parallel with viscous effects. Both types of mechanism use the same kinematic variable ε , as does the Kelvin-Voigt model (Aklonis et al. 1983), with the main difference that here the elasticity and viscosity parameters depend on T and \tilde{f} . In the literature, more general models, than the Kelvin-Voigt one, are mentioned, namely the Generalized Maxwell model which allows one to consider the evolution of E' and E'' via a multitude of viscoelastic branches placed in parallel (Aklonis et al. 1983). For each viscoelastic branch, a viscous strain is necessarily introduced as a state variable. For simplicity in what follows, we have tried to stay as close as possible to the rheological Eqs. (1) of the DMTA.

3.3.1 Thermoelastic effects

a Modeling aspects

The regular and periodic thermal oscillations, henceforth referred to as $(\delta\theta_e^{f_0})_{exp}$ (i.e., experimentally observed), led us to introduce thermoelastic effects. In this context, we proposed to rewrite Eq. (6a) in the following form:

$$\sigma^r = E'(T, f_0) (\varepsilon - \lambda_{th}\theta), \quad (8)$$

where λ_{th} is the coefficient of thermal expansion. For a thermoelastic material, this strong thermomechanical interaction results in the existence of a coupling heat source written as (Chrysochoos 2012):

$$w_{the}^{\bullet} = T \frac{\partial^2 \psi}{\partial T \partial \varepsilon} \dot{\varepsilon} + T \frac{\partial^2 \psi}{\partial T \partial \tilde{f}} \dot{\tilde{f}} = T \frac{\partial \sigma^r}{\partial T} \dot{\varepsilon} = -\lambda_{th} T E' \dot{\varepsilon} - \frac{dE'}{dT} (\varepsilon - \lambda_{th} \theta) \dot{\varepsilon}. \quad (9)$$

The notation $(-)^{\bullet}$ means that the rate of $(-)$ depends on the thermodynamic path followed. In other words, $(-)$ is not a state function. Note that the term in $\dot{\tilde{f}}$ vanishes for any monochromatic cycle ($\tilde{f} = f_0$) so that w_{the}^{\bullet} decomposes into two. The first term is well known. It causes a material to expand when heated or to cool when stretched. The second term is due to the variation of E' with the temperature. If we admit that the derivative $\frac{dE'}{dT}$ remains constant during a DMTA test, the corresponding source should beat at $2f_0$, since ε , $\dot{\varepsilon}$, and, to a good approximation θ , beat at f_0 (see above for instance in Figure 6(a)). Indeed, from an experimental standpoint, it was not possible, as shown below, to experimentally see any component of the thermo-signal beating at the frequency $2f_0$, which should have been the case if the second source term had a large amplitude. This is the reason why we have considered, in what follows, a thermoelastic source reduced to the first term:

$$w_{the}^{\bullet} \approx -\lambda_{th} T_0 E' (T_0, f_0) \dot{\varepsilon}. \quad (10)$$

To pass from heat sources to temperature variations, the heat diffusion equation is required. For simplicity, we have used in the following a differential version of the heat diffusion equation valid for homogeneous tests when the boundary heat exchange conditions are linear (Fourier conditions) (Chrysochoos et al. 2000). In such a context, the volume heat losses by conduction were modeled by a linear term in temperature variation weighted by a time constant of heat losses τ_{th} . When only the thermoelastic source is considered, this heat equation can be written as (Boulanger et al. 2004):

$$\frac{d\theta}{dt} + \frac{\theta}{\tau_{th}} = \frac{w_{the}^{\bullet}}{\rho C}, \quad (11)$$

where ρ is the mass density and C the specific heat of the material. The time constant τ_{th} can be experimentally identified for each material measuring the thermal disequilibrium $T - T_0$ over time during a given thermal loading $T_0(t)$. During these thermal loading, it was assumed that no heat source was present in the second member of Eq. (11). Figure 7 shows an illustration of the quality of the inverse identification procedure. The identified values were $\tau_{th} = 48$ s for PS and $\tau_{th} = 34$ s for PA6.6.

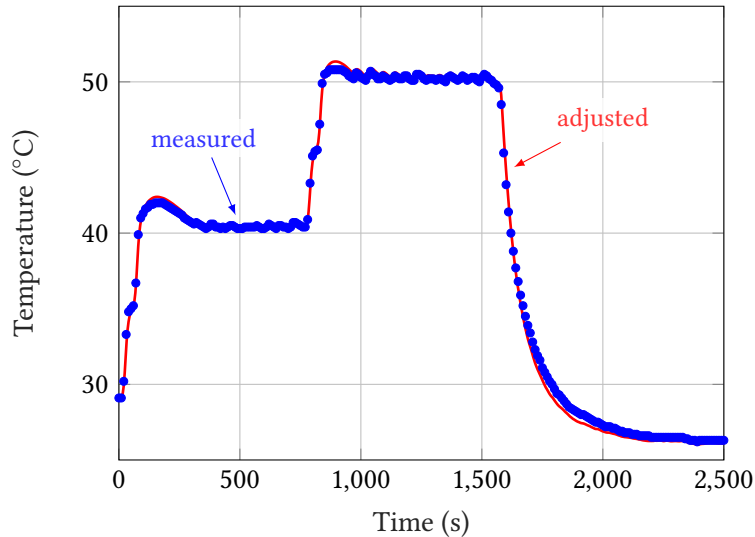


Figure 7: Measured and adjusted temperature for the estimation of τ_{th} for PS sample

The integration of Eq. (11) with thermoelastic source defined in Eq. (10), gives, once the transient terms have vanished:

$$\theta_{the}(t) = - \underbrace{\frac{\omega_0 \tau_{th}}{\sqrt{1 + \omega_0^2 \tau_{th}^2}}}_{\chi(\omega_0)} \frac{\lambda_{th} T_0 E'}{\rho C} \varepsilon_0 \sin(\omega_0 t + \phi_{the}), \quad (12)$$

where $\tan \phi_{the} = 1/(\omega_0 \tau_{th})$. The amplitude of thermal oscillations of thermoelastic origin $\delta\theta_e^{f_0}$ can therefore be related to the strain amplitude ε_0 by the relationship:

$$\left(\delta\theta_e^{f_0}\right)_{theo} = \chi(\omega_0) \frac{\lambda_{th} T_0}{\rho C} E' \varepsilon_0. \quad (13)$$

As soon as $\omega_0 \tau_{th}$ becomes larger than 1 (e.g., high frequency test, high time constant of heat losses which means that over one cycle duration, the test can be considered as adiabatic), $\chi \approx 1$ and the above expression can be simplified in $\left(\delta\theta_e^{f_0}\right)_{theo} = \frac{\lambda_{th} T_0}{\rho C} E' \varepsilon_0$. This last expression is often used in the field of thermal stress analysis (Dulieu-Barton et al. 1998), since $E' \varepsilon_0$ roughly represents the stress amplitude σ_0 . Indeed, noting that σ_0 is reached when the stress rate cancels, it can be shown from Eq. (1b) that:

$$\sigma_0 = E' \varepsilon_0 \sqrt{1 + \left(\frac{E''}{E'}\right)^2} = \frac{E' \varepsilon_0}{\sin(\arctan(\frac{E''}{E'}))}, \quad (14)$$

which remains close to $E' \varepsilon_0$ if the ratio $\frac{E''}{E'}$ remains very small compared to 1, which has been the case for the two studied materials.

b Confrontation of experimental data with predicted ones

Using Eq. (13), a mechanical estimate of $\left(\delta\theta_e^{f_0}\right)_{theo}$ has been performed for each DMTA test characterized by a (T_0, f_0) couple and compared with the experimental one $\left(\delta\theta_e^{f_0}\right)_{exp}$ obtained by using a synchronous demodulation of the signal $\theta(t)$.

To check the efficiency of the synchronous demodulation to estimate $\left(\delta\theta_e^{f_0}\right)_{exp}$, we compared the difference $\theta(t) - \tilde{\theta}(t)$ with the signal $\left(\delta\theta_e^{f_0}\right)_{exp} \sin(\omega_0 t + \phi_e)$, where ϕ_e is the phase shift of the temperature signal with the carrier signal. As an example, both signals were partly plotted in Figure 8 in the case the test shown in Figure 6(a) from $t = 85$ s to $t = 110$ s.

We also performed a synchronous demodulation of the thermo-signal $\theta(t)$ at $2f_0$, to check if the amplitude $\left(\delta\theta_e^{2f_0}\right)_{exp}$ of $\theta(t)$ induced by the 2nd term of the thermoelastic heat source was significant or not.

The mechanical and thermal data processing was therefore carried out following tests performed on the two materials at different ambient temperatures T_0 and different loading frequencies f_0 . The corresponding results were gathered in Table 2 for the PS and Table 3 for the PA6.6.

Tables 2 and 3 show that the observed thermoelastic effects are rather correctly predicted by Eq. (13). Note that, to compute the predictions of the thermoelastic model, E' assessments were used as well as values of several thermophysical parameters characterizing the material. These values are gathered in Table 4. Thermal expansion coefficient and specific heat values were extracted from the technical literature. These values may vary slightly from one reference to another, sometimes due to difference in molecular weight.

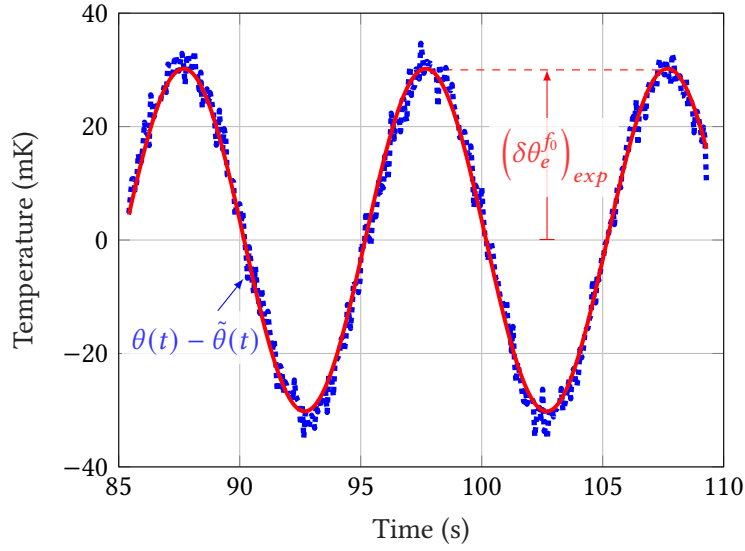


Figure 8: Efficiency of the synchronous demodulation to reach $(\delta\theta_e^{f_0})_{exp}$ (PA6.6, $T_0 = 313$ K, $f_0 = 0.1$ Hz, Figure 6(a))

f_0	T_0	E'	χ	$(\delta\theta_e^{f_0})_{theo}$	$(\delta\theta_e^{f_0})_{exp}$	$(\delta\theta_e^{2f_0})_{exp}$
[Hz]	[K]	[MPa]	[-]	[mK]	[mK]	[mK]
0.1	313	3490	0.999	51.5	45.3	1.1
1	313	3560	1.0	52.6	48.0	0.3
10	313	3610	1.0	53.3	42.8	2.4
0.1	348	2880	0.999	47.3	41.4	0.9
1	348	2980	1.0	48.9	42.0	0.6
10	348	3050	1.0	50.0	40.5	0.9
0.1	363	2530	0.999	43.3	41.8	1.6
1	363	2670	1.0	45.8	41.5	0.3

Table 2: Temperature variations induced by thermoelasticity for PS. Comparison of measured amplitudes $(\delta\theta_e^{f_0})_{exp}$ with the predictions of the thermoelastic model $(\delta\theta_e^{f_0})_{theo}$. Estimates for $(\delta\theta_e^{2f_0})_{exp}$ are not significant

f_0	T_0	E'	χ	$(\delta\theta_e^{f_0})_{theo}$	$(\delta\theta_e^{f_0})_{exp}$	$(\delta\theta_e^{2f_0})_{exp}$
[Hz]	[K]	[MPa]	[-]	[mK]	[mK]	[mK]
0.1	313	3140	0.999	40.6	30.2	0.3
1	313	3230	1.0	41.9	27.0	0.2
10	313	3290	1.0	42.7	30.0	0.1
0.1	323	2650	0.999	35.5	28.7	0.5
1	323	2850	1.0	38.1	26.6	0.0
10	323	2990	1.0	40.0	30.4	0.9
0.1	333	1920	0.999	26.4	24.4	0.2
1	333	2210	1.0	30.5	23.2	0.0

Table 3: Temperature variations induced by thermoelasticity for PA6.6. Comparison of measured amplitudes $(\delta\theta_e^{f_0})_{exp}$ with the predictions of the thermoelastic model $(\delta\theta_e^{f_0})_{theo}$. Estimates for $(\delta\theta_e^{2f_0})_{exp}$ are not significant

	ρ [kg m ⁻³]	C [J kg ⁻¹ K ⁻¹]	λ_{th} [10 ⁵ K ⁻¹]
PS	1060	1400	7.0
PA6.6	1140	1800	8.5

Table 4: Thermophysical parameters of PS and PA6.6

c Partial concluding comments

The comments that can be drawn from this data analysis are:

- Regarding the thermoelastic couplings induced by the variation of the storage modulus, i.e., $-\frac{dE'}{dT} (\varepsilon - \lambda_{th}\theta) \dot{\varepsilon}$ in Eq. (9), they remained undetectable. The values of $(\delta\theta_e^{2f_0})_{exp}$ shown in Tables 2 and 3 are too low to be significant.
- Thermoelastic effects induced by material expansion occur during a DMTA test and should probably be considered in the rheological equations. Indeed, it is possible to introduce thermoelastic contributions E'_T and E''_T to dynamic moduli considering the coupling effects beating at the loading frequency f_0 . Using Eqs. (6b), (8) and (12), we then get:

$$\left\{ \begin{array}{l} E' = E'_M + E'_{\mathcal{T}} = E'_M + \frac{\lambda_{th}^2 T_0 E_M'^2}{\rho C} \frac{\omega_0^2 \tau_{th}^2}{1 + \omega_0^2 \tau_{th}^2}, \\ E'' = E''_M + E''_{\mathcal{T}} = E''_M + \frac{\lambda_{th}^2 T_0 E_M'^2}{\rho C} \frac{\omega_0 \tau_{th}}{1 + \omega_0^2 \tau_{th}^2}. \end{array} \right. \quad (15a)$$

$$\left\{ \begin{array}{l} E' = E'_M + E'_{\mathcal{T}} = E'_M + \frac{\lambda_{th}^2 T_0 E_M'^2}{\rho C} \frac{\omega_0^2 \tau_{th}^2}{1 + \omega_0^2 \tau_{th}^2}, \\ E'' = E''_M + E''_{\mathcal{T}} = E''_M + \frac{\lambda_{th}^2 T_0 E_M'^2}{\rho C} \frac{\omega_0 \tau_{th}}{1 + \omega_0^2 \tau_{th}^2}. \end{array} \right. \quad (15b)$$

f_0	T_0	E'	E''	$E'_{\mathcal{T}}$	$E''_{\mathcal{T}}$
[Hz]	[K]	[MPa]	[MPa]	[MPa]	[MPa]
0.1	313	3490	67	12.6	0.42
1	313	3564	65	13.1	0.04
10	313	3608	64	13.5	0.00
0.1	348	2882	86	9.5	0.32
1	348	2977	77	10.2	0.03
10	348	3046	73	10.7	0.00
0.1	363	2529	140	7.7	0.25
1	363	2673	86	8.6	0.03
10	363	2826	39	9.6	0.00

Table 5: Thermoelastic contributions $E'_{\mathcal{T}}$ and $E''_{\mathcal{T}}$ to dynamic moduli of PS samples

Tables 5 and 6 show that the thermoelastic contributions to E' and E'' remained weak, particularly at high frequency. Indeed, at high frequency, the heat losses per cycle drastically decrease and the thermoelastic deformation process becomes adiabatic (no thermal dissipation). Conversely, at low or even very low frequency, we know that the loss moduli E'' tend towards zero, so we can question the relative importance of thermoelastic effects even if, at very low frequencies, the deformation process tends towards an isothermal process. From an experimental standpoint, these low frequencies are beyond the reach of the infrared techniques currently used. Nevertheless, numerical tests can be performed. We used for example a Zener-type thermoelastic model to check the possible preponderance of thermoelastic effects at low frequencies. The corresponding results will be shown in subsection 3.3.5 once the dissipative effects and energy balances have been introduced and analyzed.

3.3.2 Dissipative effects

a Modeling aspects

f_0	T_0	E'	E''	$E'_{\mathcal{T}}$	$E''_{\mathcal{T}}$
[Hz]	[K]	[MPa]	[MPa]	[MPa]	[MPa]
0.1	313	3137	85	10.8	0.51
1	313	3228	60	11.5	0.05
10	313	3292	39	11.9	0.01
0.1	323	2653	167	8.0	0.37
1	323	2850	119	9.2	0.04
10	323	2992	76	10.2	0.00
0.1	333	1920	211	4.3	0.20
1	333	2211	195	5.7	0.03
10	333	2497	151	7.3	0.00

Table 6: Thermoelastic contributions $E'_{\mathcal{T}}$ and $E''_{\mathcal{T}}$ to dynamic moduli of PA6.6 samples

The irreversible character of the deformation process is expressed by the Clausius-Duhem inequality. In the framework of DMTA tests, with the chosen set of state variables, the dissipation d can be written as:

$$d = \underbrace{\sigma \dot{\varepsilon} - \frac{\partial \psi}{\partial \varepsilon} \dot{\varepsilon} - \frac{\partial \psi}{\partial \tilde{f}} \dot{\tilde{f}}}_{d_1} - \underbrace{\frac{\overrightarrow{\text{grad}} T}{T} \cdot \vec{q}}_{d_2} \geq 0. \quad (16)$$

This dissipation is traditionally split in two terms: the intrinsic dissipation denoted by d_1 and the thermal dissipation d_2 . In Eq. (16), \vec{q} is the heat influx vector. The thermal dissipation d_2 depicts the irreversibility related to the heat diffusion mechanisms. In general, the Fourier law is used to link the heat influx vector to the temperature field. Fourier's law is classically written as:

$$\vec{q} = -k \overrightarrow{\text{grad}} T, \quad (17)$$

where k is the conduction tensor. In the 1D rheological context of DMTA tests, the irreversibility induced by heat diffusion has been considered via the heat losses term θ/τ_{th} present in the simplified heat equation, Eq. (11). Recall that the existence of heat losses (i.e., neither isothermal nor adiabatic test) in the presence of coupling mechanisms (e.g., thermoelasticity), leads to time effects that, during a cyclic test, contributes to form a hysteresis loop (Chrysochoos 2012). This effect was highlighted by Zener in his work (Zener 1938) introducing the famous concept of thermoelastic internal friction.

The intrinsic dissipation d_1 depicts the mechanical and microstructural irreversibility. Considering Eqs. (6a) and (6b) the constancy of the variable \tilde{f} for a monochromatic test, d_1 can be rewritten in the following compact form:

$$d_1 = \sigma^{ir} \dot{\varepsilon} = \frac{E''_{\mathcal{M}}}{\omega_0} \dot{\varepsilon}^2 = E''_{\mathcal{M}} \omega_0 \varepsilon_0^2 \cos^2(\omega_0 t) = E''_{\mathcal{M}} \omega_0 \varepsilon_0^2 \frac{1 + \cos(2\omega_0 t)}{2} \geq 0. \quad (18)$$

This term corresponds to the part of the deformation energy rate $\sigma \dot{\varepsilon}$ that is attributed to the loss modulus. The thermodynamic analysis allows one to claim that this mechanical energy rate is dissipated and must therefore be irreversibly transformed into heat. To check the coherence of this interpretation from a dissipative standpoint with the experimental results, the following way has been chosen.

The goal is to pass from dissipation to self-heating temperature. Analogously to Eq. (11), the heat diffusion equation considering the dissipative source only was rewritten as:

$$\frac{d\theta}{dt} + \frac{\theta}{\tau_{th}} = \frac{d_1}{\rho C}. \quad (19)$$

Then, using the analytic form of the intrinsic dissipation given in Eq. (18), the heat equation was integrated over time to give the evolution of the corresponding thermal effects. Let us note θ_d the temperature variation, solution of Eq. (19). Once the transient term vanished, we have got:

$$\theta_d(t) = \left(\frac{1}{2} + \frac{1}{\sqrt{1 + 4\omega_0^2 \tau_{th}^2}} \sin(2\omega_0 t + \phi_d) \right) \frac{E''_M \varepsilon_0^2 \omega_0 \tau_{th}}{\rho C}, \quad (20)$$

with $\tan(\phi_d) = \frac{1}{2\omega_0 \tau_{th}}$.

The non-inclusion of the transient term in Eq. (20) does not pose any problem, for the confrontation between theoretical predictions and experimental results, because the experimental estimate of the temperature variations is made comparing the temperature of the strained sample with a non-loaded one. Note that, once again, a component of the thermo-signal should beat at $2f_0$. However, the weighting term in front of it tends very quickly to zero for f_0 greater than 10^{-1} Hz in the present case, and more generally when $f_0 \gg \frac{1}{2\pi\tau_{th}}$.

Whatever the frequency f_0 , the mean temperature variation θ_d stabilizes around the value $(\delta\theta_d^{f_0})_{theo}$ defined by:

$$(\delta\theta_d^{f_0})_{theo} = \frac{E''_M \varepsilon_0^2 \omega_0 \tau_{th}}{2\rho C} = \frac{\pi E''_M \varepsilon_0^2 \tau_{th}}{\rho C} f_0. \quad (21)$$

b Confrontation of experimental data with predicted ones

The stabilized temperatures $(\delta\theta_d^{f_0})_{theo}$ were compared to the corresponding values $(\delta\theta_d^{f_0})_{exp}$ experimentally observed for each couple (T_0, f_0) . Results are gathered in Tables 7 and 8 for PS and PA6.6 samples, respectively.

f_0	T_0	E''	$(\delta\theta_d^{f_0})_{theo}$	$(\delta\theta_d^{f_0})_{exp}$
[Hz]	[K]	[MPa]	[mK]	[mK]
0.1	313	67	0.7	8.0
1	313	65	6.4	11.1
10	313	64	62.4	21.2
0.1	348	86	0.8	23.7
1	348	72	7.0	16.8
10	348	76	74.3	50.3
0.1	363	140	1.4	21.9
1	363	86	8.4	37
10	363	39	38.3	61.9

Table 7: Comparison of experimental and theoretical dissipation-induced self-heating for PS

The confrontation of "theoretical" and "experimental" dissipation-induced self-heating values may appear more delicate than the one concerning thermoelastic effects. In the previous case, the synchronous demodulation technique allowed to delete almost totally the low frequency thermal noise (chamber regulation) and high frequency one (electronic noise, parasitic reflections). On the other hand, the temperature increases induced by dissipation seem much more scattered.

f_0	T_0	E''	$(\delta\theta_d^{f_0})_{theo}$	$(\delta\theta_d^{f_0})_{exp}$
[Hz]	[K]	[MPa]	[mK]	[mK]
0.1	313	85	0.4	-1.0
1	313	60	3.1	10.0
10	313	39	20.3	85.0
0.1	323	167	0.9	-14.8
1	323	119	6.2	23.2
10	323	76	39.4	143.4
0.1	333	211	1.1	-0.4
1	333	195	10.2	24.4
10	333	151	78.4	189.6

Table 8: Comparison of experimental and theoretical dissipation-induced self-heating for PA6.6

c Partial concluding comments

But then, what can we learn from the analysis of self-heating? For both materials, the trend is clear: the higher the loading frequency, the more the sample self-heats, at least at the loading frequencies used. At $f_0 = 0.01$ Hz, the effects of noise were however visible in that negative values of $(\delta\theta_d^{f_0})_{exp}$ are experimentally detected, especially in the case of PA6.6 samples. At high frequencies ($f_0 = 10$ Hz), the most important self-heating did not exceed 200 mK. It is worth noting that these thermal effects increase so little from one loading frequency to another. For example, it can be noticed that at 1 Hz and 10 Hz, the self-heating does not increase in a ratio of ten, but less, of the order of 2-3 for PS and 6-8 for PA6.6. At these same loading frequencies, we could have probably amplified these thermal effects by increasing the strain amplitude ε_0 which remains very low ($\varepsilon_0 = 10^{-3}$). But it seemed important to stay within a deformation range where the linear viscoelasticity framework seems to be indisputable. We came back to this important point in the final concluding comments.

3.3.3 Energy rate balance

The previous paragraphs have shown that the thermal effects induced by thermoelasticity and dissipation have comparable ranges, of the order of a hundred mK. It seemed interesting to see now what the associated heat rates correspond to. For this purpose, energy rate balances are proposed. We have chosen, this time, to show these balances for PS specimens loaded under extreme conditions (see Figures 9a-b).

The terms defining the energy balance rate are gathered in Eqs. (22a-22d). The deformation energy rate w_{def}^\bullet is made of elastic (w_e^\bullet) and dissipated (w_d^\bullet) energy rates. We also added the thermoelastic energy rate w_{the}^\bullet , even if it does not appear in the classic DMTA.

$$\left\{ \begin{array}{l} w_{def}^\bullet = \sigma \dot{\varepsilon} = w_e^\bullet + w_d^\bullet, \end{array} \right. \quad (22a)$$

$$\left\{ \begin{array}{l} w_e^\bullet = \sigma^r \dot{\varepsilon} = E'_M (\varepsilon - \lambda_{th} \theta) \dot{\varepsilon} \approx \frac{1}{2} E'_M \varepsilon_0^2 \omega_0 \sin(2\omega_0 t), \end{array} \right. \quad (22b)$$

$$\left\{ \begin{array}{l} w_d^\bullet = \sigma^{ir} \dot{\varepsilon} = E''_M \varepsilon_0^2 \omega_0 \cos^2(\omega_0 t), \end{array} \right. \quad (22c)$$

$$\left\{ \begin{array}{l} w_{the}^\bullet = -\lambda_{th} T E'_M \dot{\varepsilon} = -\lambda_{th} (T_0 + \theta) E'_M \varepsilon_0 \omega_0 \cos(\omega_0 t). \end{array} \right. \quad (22d)$$

The approximation made in Eq. (22b) comes from the fact that $\lambda_{th} \theta \ll \varepsilon$.

The first obvious result is that the thermoelastic energy rate involved in the transformation is undoubtedly the most important term of the balance. In Figure 9, it should be noted that to make the comparison of the curves easier, the thermoelastic energy rate has been divided by 25.

The second result, equally obvious, is the extreme lowness of dissipation. The dissipation is so low that the deformation energy rate is almost identical to that of the elastic one. Nevertheless, it has been underlined that these small mechanical dissipations (always positive) generated

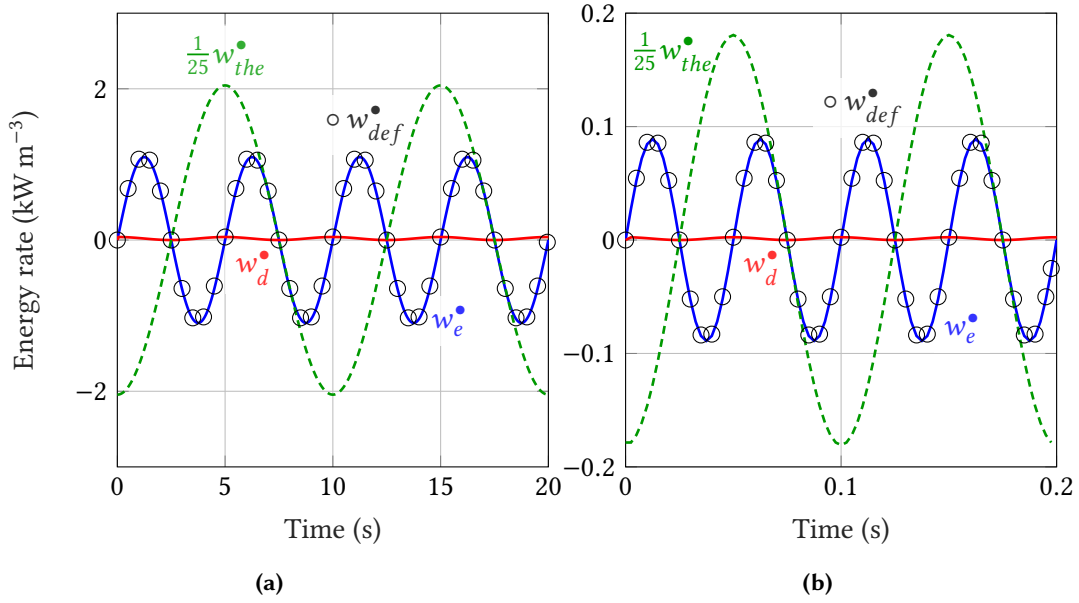


Figure 9: Energy rate balances for PS: (a) $T_0 = 313$ K, $f_0 = 0.1$ Hz; (b) $T_0 = 363$ K, $f_0 = 10$ Hz

temperature variations comparable to those induced by (alternating) thermoelastic coupling sources.

3.3.4 Hysteresis area

The energy preponderance of coupling effects led us to control the influence that their presence can have on the hysteresis loop area \mathcal{A}_h . Using Eq. (15b), we get:

$$\mathcal{A}_h = \int_t^{t+f_0^{-1}} \sigma(\tau) \dot{\varepsilon}(\tau) d\tau = \pi E'' \varepsilon_0^2 = \mathcal{A}_h^d + \mathcal{A}_h^{the}, \quad (23)$$

where \mathcal{A}_h^d and \mathcal{A}_h^{the} stand for the dissipative and the thermoelastic contributions. The viscous term \mathcal{A}_h^d is naturally defined by:

$$\mathcal{A}_h^d = \int_t^{t+f_0^{-1}} d_1(\tau) d\tau. \quad (24)$$

The presence of strong thermomechanical coupling mechanisms in non-adiabatic situation, leads to time effects that contribute to the creation of a hysteresis loop. In the case of thermoelastic effects, this contribution \mathcal{A}_h^{the} is written as, using Eq. (12):

$$\mathcal{A}_h^{the} = \int_t^{t+f_0^{-1}} w_{the}^{\bullet} d\tau = \int_t^{t+f_0^{-1}} \underbrace{-E'_{\mathcal{M}} \lambda_{th} \left(\delta \theta_e^{f_0} \right)_{theo}}_{\theta_{the}(\tau)} \underbrace{\sin(\omega_0 \tau + \phi_{the}) \varepsilon_0 \omega \cos(\omega_0 \tau)}_{\dot{\varepsilon}(\tau)} d\tau. \quad (25)$$

Then, after integration over time, we get:

$$\mathcal{A}_h^{the} = \frac{\pi E'_{\mathcal{M}} \varepsilon_0 \lambda_{th} \left(\delta \theta_e^{f_0} \right)_{theo}}{\sqrt{1 + \omega_0^2 \tau_{th}^2}} = \pi E''_{\mathcal{T}} \varepsilon_0^2. \quad (26)$$

In Tables 9 and 10 both types of hysteresis areas have been computed.

The remarkable finding is that despite the preponderance of thermoelastic effects in the energy rate balance, the contribution of these coupling effects to the creation of a hysteresis area

f_0	T_0	E'	E''	$(\delta\theta_e^{f_0})_{exp}$	\mathcal{A}_h	\mathcal{A}_h^{the}
(Hz)	(K)	(MPa)	(MPa)	(mK)	(J m ⁻³)	(J m ⁻³)
0.1	313	3490	67	51.5	210	1.85
1	313	3564	65	52.6	205	0.19
10	313	3608	64	53.3	199	0.02
0.1	348	2882	86	47.3	269	1.40
1	348	2977	77	48.9	242	0.15
10	348	3046	73	50.0	229	0.02
0.1	363	2529	140	43.3	441	1.13
1	363	2673	86	45.8	269	0.13
10	363	2826	39	48.4	123	0.01

Table 9: Computations of the hysteresis area \mathcal{A}_h and \mathcal{A}_h^{the} for DMTA tests on PS samples

f_0	T_0	E'	E''	$(\delta\theta_e^{f_0})_{exp}$	\mathcal{A}_h	\mathcal{A}_h^{the}
(Hz)	(K)	(MPa)	(MPa)	(mK)	(J m ⁻³)	(J m ⁻³)
0.1	313	3137	85	41	267	1,61
1	313	3228	60	42	187	0,17
10	313	3292	39	43	122	0,02
0.1	323	2653	167	35	526	1,16
1	323	2850	119	38	375	0,14
10	323	2992	76	40	238	0,01
0.1	333	1920	211	26	663	0,62
1	333	2211	195	30	614	0,08
10	333	2497	151	34	474	0,01

Table 10: Computations of the hysteresis area \mathcal{A}_h and \mathcal{A}_h^{the} for DMTA tests on PA6.6 samples

remains negligible in the loading conditions considered here, particularly at high frequency. This is the same type of conclusion obtained when studying the influence of thermoelastic effects on the definition of dynamic moduli (see Eq. (15b) and Tables 5 and 6). But, as announced in Subsection 3.3.1, we sought to see if coupling effects still have as little relative importance on the size of hysteresis loop at very low frequencies. In other words, at very low frequencies, is irreversibility associated with intrinsic or thermal dissipation, viscosity or material thermo-dilatatability?

3.3.5 Possible extrapolation to very low frequencies

Since the thermal effects at very low loading frequencies are experimentally unreachable, numerical simulations were performed using a basic visco-thermo-elastic Zener-type model (Fig. 10) (see Moreau et al. (2005)). The parameters used in the simulations are listed in Table 11. The values of thermal expansion coefficient λ_{th} , of the mass density ρ , of the specific heat C were the ones retained for the PS samples. The elastic moduli E_1 and E_2 and the viscosity μ_2 were chosen to get the same hysteresis area \mathcal{A}_h and \mathcal{A}_h^{the} obtained for PS samples at $T_0 = 363$ K, $f_0 = 0.1$ Hz (see bold line in Table 12). We also made sure that the chosen E_1 , E_2 and μ_2 give dynamic moduli that follow as well as possible their experimental evolutions with f_0 at T_0 . At best only, because the euristic Zener model, which has only one thermoelastic and one viscoelastic branch, remains a rather simple model.

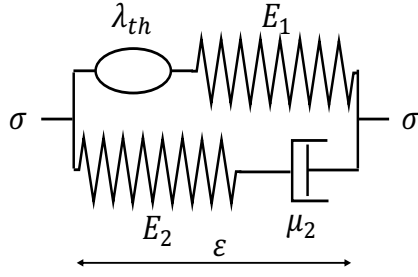


Figure 10: Basic sketch of the Zener-type rheological model

Parameters	Values
E_1 [MPa]	2500
E_2 [MPa]	620
μ_2 [MPa s]	241
τ_2 [s]	0.39
λ_{th} [10^{-6}K^{-1}]	75
ρ [kg m^{-3}]	1060
C [$\text{J kg}^{-1} \text{K}^{-1}$]	1400
τ_{th} [s]	40
ε_0 [-]	0.01

Table 11: Values of the model parameters used in the numerical simulations

The energies \mathcal{A}_h and \mathcal{A}_h^{the} were computed for different low frequencies and gathered in Table 12. As the loading frequency decreases, the contribution of thermoelastic effects to the hysteresis area $\mathcal{R} = \frac{\mathcal{A}_h^{the}}{\mathcal{A}_h} = \frac{E''}{E'}$ increases. In Table 12, we see that the ratio \mathcal{R} tends numerically to a limit value when the loading frequency tends to zero. An analytical calculation of the ratio associated with the thermoelastic model of Zener type, gives a limit value equal to:

$$\lim_{f_0 \rightarrow 0} \mathcal{R} = \frac{E_1^2 \lambda_{th}^2 T_0 \tau_{th}}{E_1^2 \lambda_{th}^2 T_0 \tau_{th} + \rho C \mu_2} = 0.588. \quad (27)$$

This result can be easily obtained using the expression of the dynamic moduli associated with the Zener-type model. We classically get:

$$\begin{cases} E' = E_1 + E_2 \frac{\omega_0^2 \tau_2^2}{1 + \omega_0^2 \tau_2^2}, \\ E'' = E_2 \frac{\omega_0 \tau_2}{1 + \omega_0^2 \tau_2^2}, \end{cases} \quad (28a)$$

$$(28b)$$

where $\tau_2 = \frac{\mu_2}{E_2}$ is the relaxation time of the viscoelastic branch.

f_0	\mathcal{A}_h^d	\mathcal{A}_h^{the}	\mathcal{R}
[Hz]	[J m^{-3}]	[J m^{-3}]	[%]
10^{-4}	0.47	0.68	58.7
10^{-3}	4.7	6.3	56.9
10^{-2}	47.3	9.1	16.2
10^{-1}	441	1.1	0.25
10^0	669	0.12	0.02
10^1	79.7	0.01	0.015
10^2	8.0	0.001	0.015

Table 12: Relative importance of thermoelastic effects at different loading frequencies

At very low frequencies, for the material characteristics selected here, the preponderance of the thermoelastic effects is then indisputable. This means that, at these frequencies, the loss modulus is preferentially induced by thermomechanical coupling effects associated with heat diffusion rather than viscous effects. One could introduce at this level the concept of "coupling viscosity" μ_c induced by the thermo-dilatibility character of the material in a non-adiabatic, non-isothermal context. At very low frequencies, the thermoelastic effects will be more important than viscous effects if the "coupling viscosity" is greater than the material viscosity:

$$\mu_c = \frac{E_1^2 \lambda_{th}^2 T_0 \tau_{th}}{\rho C} > \mu_2. \quad (29)$$

In Table 12, one can also notice the non-monotonic evolution of \mathcal{A}_h^{the} when the loading frequency f_0 increases, following a passage from isothermal (i.e., low frequencies) to adiabatic (i.e., high frequencies) processes.

4 Concluding comments

In this work, we first sought to develop with an infrared device allowing to reach the very small temperature variations accompanying the cyclic loading of polymer samples during DMTA tests. The first important finding, in agreement with the DMTA interpretation framework, is that the temperature variations of the specimen during the tests remain so small that the assumption of isothermal testing is well acceptable from a purely thermal standpoint, but not necessarily from an energy standpoint since, for solid materials (high mass density, high specific heat), a small thermal effect can reveal important energy mechanisms.

To interpret the thermomechanical results and their energy consequences, we integrated the rheological equations of the DMTA in the framework of the nonlinear TIP with internal state variables.

The thermodynamic analysis of mechanical and thermal data, obtained during various loading frequencies and temperatures, led us first to justify the introduction of thermoelastic effects. As far as thermoelasticity is concerned, (i) its temperature ranges have been of the same order of magnitude as those induced by viscous effects, (ii) it was very largely preponderant within the energy rate balance, (iii) but unexpectedly and fortunately its contribution to the mechanical hysteresis area remained negligible in the loading conditions experimentally considered. However, at very low frequencies, numerical predictions from a Zener-type model showed that, depending on the material characteristics, the loss modulus might be preferentially attributed to coupling effects rather than viscous effects.

As for the dissipative effects: (i) they were more difficult to observe because the intensity of dissipation remained extremely low (more than 100 times lower than the thermoelastic energy rates), (ii) we could nevertheless highlight that the dissipation increased with the loading frequency but in a proportion lower than the ratio of the frequencies, (iii) this last result is certainly to be refined but it agrees with the fact that the area of the mechanical hysteresis loops decreases with the loading frequency. This result is also compatible with the predictions of the Generalized Maxwell model, at least if the equivalent viscosity remains a sufficiently decreasing function of the loading frequency. Indeed, if $E_1(T_0), \dots, E_i(T_0), \dots, E_{n-1}(T_0), E_n(T_0)$ denote the elastic moduli and $\mu_1(T_0), \mu_2(T_0), \dots, \mu_i(T_0), \dots, \mu_n(T_0)$, the viscosity coefficients of these n viscoelastic branches placed in parallel (with $E_n(T_0) = \infty$ and $\mu_1(T_0) = \infty$), it is classically shown (Ferry 1980) that the equivalent loss modulus E'' can be written as:

$$E'' = \left(\sum_{i=2}^n \frac{\mu_i(T_0)}{1 + \tau_i^2 \omega_0^2} + \mu_n(T_0) \right) \omega_0, \quad (30)$$

according to Eq. (23), the hysteresis area \mathcal{A}_h is therefore written:

$$\mathcal{A}_h = \underbrace{\left(\sum_{i=2}^n \frac{\mu_i(T_0)}{1 + \tau_i^2 \omega_0^2} + \mu_n(T_0) \right)}_{\mu_{eq}(T_0, f_0)} 2\pi^2 \varepsilon_0^2 f_0, \quad (31)$$

where $\tau_i(T_0) = \frac{\mu_i(T_0)}{E_i(T_0)}$ is the relaxation time associated with branch $\#i$. As long as the apparent viscosity $\mu_{eq}(T_0, f_0)$ is frequency dependent, a decay of the hysteresis area with the loading frequency is possible, but once the asymptotic value $\mu_{eq}(T_0, f_0) = \mu_n(T_0)$ is reached, the hysteresis

loop area must become an increasing linear function of f_0 . It seems then difficult to interpret the near constancy of E'' observed on the PS at 333 K (see Fig. 4). This constancy would tend to show that only the viscous (pure) branch is active its viscosity μ_n evolving in f_0^{-1} , which is not consistent with the framework of linear viscoelasticity. This will be discussed in more detail in a future work, where we will seek to identify from the DMTA results on PS and PA6.6, a possibly non-linear generalized Maxwell model taking the thermoelasticity into account.

References

- Aklonis, J. J. and W. J. Mac Knight (1983). *Introduction to polymer viscoelasticity*. 2. Wiley-Interscience
- Batsale, J.-C., A. Chrysochoos, H. Pron, and B. Wattrisse (2013). "Thermographic analysis of material behaviors". *Full field Measurements and identification in solid mechanics*. Wiley. Chap. 16, pp. 467–496. DOI: [10.1002/9781118578469.ch16](https://doi.org/10.1002/9781118578469.ch16)
- Boulangier, T., A. Chrysochoos, C. Mabru, and A. Galtier (2004). "Calorimetric analysis of dissipative and thermoelastic effects associated with the fatigue behavior of steels". *International Journal of Fatigue* 26 (3), pp. 221–229. DOI: [10.1016/S0142-1123\(03\)00171-3](https://doi.org/10.1016/S0142-1123(03)00171-3)
- Chrysochoos, A. (2012). "Thermomechanical analysis of the cyclic behavior of materials". *Procedia IUTAM* 4, pp. 15–26. DOI: [10.1016/j.piutam.2012.05.003](https://doi.org/10.1016/j.piutam.2012.05.003)
- Chrysochoos, A. and H. Louche (2000). "An infrared image processing to analyse the calorific effects accompanying strain localisation". *International Journal of Engineering Science* 38 (16), pp. 1759–1788. DOI: [10.1016/S0020-7225\(00\)00002-1](https://doi.org/10.1016/S0020-7225(00)00002-1)
- Dulieu-Barton, J. M. and P. Stanley (1998). "Development and applications of thermoelastic stress analysis". *The Journal of Strain Analysis for Engineering Design* 33 (2), pp. 93–104. DOI: [10.1243/0309324981512841](https://doi.org/10.1243/0309324981512841)
- Ferry, J. D. (1980). *Viscoelastic properties of polymers*. 3. John Wiley & Sons
- Germain, P., P. Suquet, and Q. S. Nguyen (1983). "Continuum thermodynamics". *Journal of Applied Mechanics* 50 (4b), pp. 1010–1020
- Graessley, W. W. and L. J. Fetters (2001). "Thermoelasticity of Polymer Networks". *Macromolecules* 34.20, pp. 7147–7151. DOI: [10.1021/ma010989p](https://doi.org/10.1021/ma010989p)
- Halphen, B. and Q. S. Nguyen (1975). "Sur les matériaux standard généralisés". *Journal de Mécanique* 14.1, pp. 39–63
- Honorat, V., S. Moreau, J.-M. Muracciole, B. Wattrisse, and A. Chrysochoos (2005). "Calorimetric analysis of polymer behaviour using a pixel calibration of an IRFPA camera". *Quantitative InfraRed Thermography Journal* 2.2, pp. 153–171. DOI: [10.3166/qirt.2.153-171](https://doi.org/10.3166/qirt.2.153-171)
- Menard, K. P. (2008). *Dynamic Mechanical Analysis: A practical introduction*. 2. CRC Press. DOI: [10.1201/9781420053135](https://doi.org/10.1201/9781420053135)
- Moreau, S., A. Chrysochoos, J.-M. Muracciole, and B. Wattrisse (2005). "Analysis of thermoelastic effects accompanying the deformation of PMMA and PC polymers". *Comptes Rendus Mécanique* 333.8, pp. 648–653. DOI: [10.1016/j.crme.2005.06.007](https://doi.org/10.1016/j.crme.2005.06.007)
- Olusanya, A. (1996). "A comparison of techniques for monitoring the cure of adhesives". *National Physical Laboratory Report CMMT (B)*, p. 104
- Sokolov, A. P. and Y. Hayashi (2007). "Breakdown of time-temperature superposition: From experiment to the coupling model and beyond". *Journal of Non-Crystalline Solids* 353 (41), pp. 3838–3844. DOI: [10.1016/j.jnoncrysol.2007.02.063](https://doi.org/10.1016/j.jnoncrysol.2007.02.063)
- Treloar, L. R. (2005). *The physics of rubber elasticity*. 3. Oxford University Press
- Wattrisse, B., A. Chrysochoos, J.-M. Muracciole, and M. Némoz-Gaillard (2001). "Analysis of strain localization during tensile tests by digital image correlation". *Experimental Mechanics* 41, 29–39
- Yadav, P. (2019). "Time and thermo-mechanical coupling effects in polymers". Université de Montpellier
- Zener, C. (1938). "Internal friction in solids II. general theory of thermoelastic internal friction". *Physical Review* 53 (1), p. 90. DOI: [10.1103/PhysRev.53.90](https://doi.org/10.1103/PhysRev.53.90)